Precise and versatile microplate reader-based analyses of biosensor signals from arrayed microbial colonies

Fabian S. F. Hartmann[1, #], Tamara Weiß[1, #], Louise L. B. Kastberg[1], Christopher T. Workman[1], Gerd M. Seibold[1*]

[1]Section for Synthetic Biology, Department Bioengineering, Technical University of Denmark (DTU), Lyngby, Denmark

[#]These authors have contributed equally to this work and share first authorship

***Correspondence:** Gerd M. Seibold, Section of Synthetic Biology, Department of Biotechnology and Biomedicine, Technical University of Denmark, Søltofts Plads Building 223, DK-2800, Kongens Lyngby, Denmark; e-mail: gesei@dtu.dk

Keywords: Lab-automation, Mrx1-roGFP2, mCherry, GFP, arrayed microbial colonies, genetically encoded biosensors

Abstract

Genetically encoded fluorescent biosensors have emerged as a powerful tool to support phenotypic screenings of microbes. Optical analyses of fluorescent sensor signals from colonies grown on solid media can be challenging as imaging devices need to be equipped with appropriate filters matching the properties of fluorescent biosensors. Towards versatile fluorescence analyses of different types of biosensor signals derived from arrayed colonies, we investigate here the use of monochromator equipped microplate readers as an alternative to imaging approaches. Indeed, for analyses of the LacI-controlled expression of the reporter mCherry in *Corynebacterium glutamicum,* or promoter activity using GFP as reporter in *Saccharomyces cerevisiae*, an improved sensitivity and dynamic range was observed for a microplate reader-based analyses compared to their analyses *via* imaging. The microplate reader allowed us to capture signals of ratiometric fluorescent reporter proteins (FRPs) with a high sensitivity and thereby to further improve the analysis of internal pH via the pH-sensitive FRP mCherryEA in *Escherichia coli* colonies. Applicability of this novel technique was further demonstrated by assessing redox states in *C. glutamicum* colonies using the FRP Mrx1-roGFP2. By the use of a microplate reader, oxidative redox shifts were measured in a mutant strain lacking the non-enzymatic antioxidant mycothiol (MSH), indicating its major role for maintaining a reduced redox state also in colonies on agar plates. Taken together, analyses of biosensor signals from microbial colonies using a microplate reader allows comprehensive phenotypic screenings and thus facilitates further development of new strains for metabolic engineering and systems biology.

1 Introduction

Phenotypic screening of microbial strain libraries for interesting genetic variants underlies many current investigations ranging from analyses of gene functions in basic research on microbial physiology to high-throughput genetic engineering of tailor-made biotechnological platform organisms [1–4]. In the best case scenario the trait of interest is directly coupled to a phenotypic output such as growth and/or formation of a natural chromophore or fluorophore[5] allowing the easy identification of the strains of interest [6]. However, target phenotypes often cannot easily be detected and laborious analytical methods such as HPLC-analyses of metabolite levels would be required to identify interesting candidates. In these cases, genetically encoded biosensors have emerged as a valuable tool to facilitate high-throughput screenings. Such biosensors provide the advantage that an intracellular signal is transduced into an output signal, which can easily be measured from each strain of a library in a high-throughput manner[7,8]. Organisms naturally possess a variety of different types of sensors to monitor the intra- or extracellular accumulation of small molecules, ions, or changes in physical parameters. By applying synthetic biology tools, these properties can be harnessed to develop biosensors for high-throughput screenings [9]. Transcription factor-based biosensors (TFBs) represent some of the most common types of biosensors applied which are often based on metabolite-sensing transcription factors. Upon interacting with effector molecules, the expression of an actuator gene, such as a fluorescent protein, is controlled [10,11]. In contrast to TFBs, fluorescent reporter proteins (FRPs) act both as sensor and actuator. FRPs can undergo conformational changes upon interaction with a target metabolite or change in physiological state, which is subsequently accompanied by a change in their intrinsic fluorescence characteristics [12,13]. To date, many different TFBs and FRPs are available for measuring a broad range of internal metabolites or physiological states in microbial cells [12–18].

Besides the selection of specific biosensors for the screening of strain libraries, the experimental set-up also represents a major determinant to be considered for an efficient screening method. High-

69 throughput analysis of microbial libraries can be conducted in well-plates, on agar plates, via
70 fluorescence-activated cell sorting (FACS), or droplet-based screening [7]. Compared to FACS or droplet-
71 based screening approaches, screenings conducted in well-plates and on agar plates significantly lowers
72 the throughput that can be achieved. However, it provides the advantage that biosensor signals from
73 tested strain can be directly compared under various conditions [19]. Agar plate screens are considered as
74 less laborious and provide a slightly higher throughput when compared to well-plate screens. However,
75 agar plate screenings are dependent on optical readouts using camera-based imaging systems[7]. As
76 supplier-specific filters for excitation and emission are required, the flexibility for assessing different
77 fluorescent signals is low [7]. Furthermore, the fixed position of light sources and camera in the imaging
78 system affects sensitivity and might cause shadow-effects dependent of the location of the colony on
79 the agar plate [20]. In contrast, multimode plate readers equipped with monochromators and
80 photomultipliers, commonly applied for well-plate screenings, offer a high flexibility, sensitivity, and
81 easy adaptation of reader properties to the respective biosensor applied.

82 Despite the aforementioned challenges, we successfully applied the ratiometric FRP mCherryEA
83 biosensor to visualize the internal pH of *E. coli* colonies growing on agar plates measured by a FUSION FX
84 (Vilber) imaging system[8]. To adequately capture the ratiometric biosensor signals, the imaging system
85 was equipped with two capsules (excitation laser and filter module) for excitation (530 nm and 440 nm)
86 and a filter for capturing the emission (595 nm) of the pH-sensitive mCherry variant mCherryEA[8].

87 The visualization of other biosensor signals (i.e. the redox biosensor protein Mrx1-roGFP2 with an
88 excitation at 380 nm and 470 nm/ and an emission at 510 nm[16]) requires that the imaging system set-up
89 is adapted to the properties of the applied fluorescent protein. Thus, applying another fluorescent
90 protein is not readily possible if such appropriate filter modules are not available. This limitation also
91 extends to most of the widely applied imaging systems for microbial colonies, as most cannot be

92 equipped with varying and/or multiple fluorescence filter modules, and thus cannot be used to capture
93 ratiometric fluorescence signals.

94 Recently, a standard microplate reader was applied as a tool for image-based real-time gene expression
95 analysis using TFBs in living cells growing on the surface of solid media[21]. By scanning the surface of
96 rectangle OmniTray plates, fluorescence signals from organisms growing on agar allowed for imaging
97 with different resolutions (highest resolution = 360 × 240)[21]. During phenotypic screenings on agar
98 plates, strains are typically pinned from a 96-well source plate as an array of 96, 384, or 1536 colonies
99 on rectangular OmniTray plates [19]. Therefore, the positions of the arrayed colonies on the agar plates
100 are identical to the typical array of wells on conventional microplates used in microplate readers. This
101 prompted us to test standard microplate reader systems for their applicability to assess fluorescence
102 signals from arrayed colonies on agar plates.

103 In this study we demonstrate the wide applicability of microplate reader-based system to measure
104 fluorescence signals from arrayed colonies on agar plates. This method is shown for different types of
105 biosensors including a TFB based on LacI for regulated mCherry expression in *C. glutamicum*, promoter-
106 based biosensors using yeast enhanced GFP (yeGFP) as fluorescent reporter in *S. cerevisiae*, and the FRP
107 mCherryEA to assess the internal pH in *E. coli* colonies. We further show that the method developed
108 here enables the accurate measurement of redox states for *C. glutamicum* colonies via the ratiometric
109 sensor protein Mrx1-roGFP2 on agar plates.

110

2 Results and discussion

2.1 Microplate reader-based analysis of transcription factor-based biosensors in *C. glutamicum* colonies on agar plates

TFBs are widely used in microbial physiology, metabolic engineering, and synthetic biology. Many designs for TFBs include fluorescent proteins as a reporter, which provides an easy optical readout to screen for high or low fluorescent variants from a library. Genome wide screens are often conducted via arrayed colonies on agar plates, as this approach offers a higher capacity than well-plate based screens and the comparison of different conditions[7]. However, as stated above, analyses of fluorescence signals from colonies via imaging can be challenging[22].

To compare fluorescence imaging with microplate reader-based measurements, two model strains, *C. glutamicum* (pEKEx2_low-*mCherry*) and *C. glutamicum* (pEKEx2_high-*mCherry*), were constructed to compare fluorescence imaging with microplate reader-based measurements. The two strains were transformed using plasmids pEKEx2_low-*mCherry and* pEKEx2_high-*mCherry*, both consisting of the IPTG inducible promoter P_{tac} but differed in the strength of the ribosomal binding site (RBS) for expression of the reporter *mCherry* (Fig. 1a). To verify the different expression levels, C*. glutamicum* (pEKEx2_low-*mCherry*) and *C. glutamicum* (pEKEx2_high-*mCherry*) were cultivated in BHI liquid medium supplemented with different IPTG concentrations followed by endpoint fluorescence analysis using a microplate reader (SpectraMax). As depicted in Fig. 1b, both strains revealed an IPTG dose-dependent increase of the respective fluorescence intensity. As expected, the use of a stronger RBS in *C. glutamicum* (pEKEx2_high-*mCherry*) resulted in a higher maximal mCherry fluorescence level when compared to C*. glutamicum* (pEKEx2_low-*mCherry*). Moreover, no increased fluorescence levels were measured for the control strain *C. glutamicum* (pEKEx2) with an empty vector (Fig.1b). Analysis of fluorescence levels obtained under fully induced conditions (> 500 µM) revealed that fluorescence signals of all three strains were significantly different to each other. In presence of the highest tested

IPTG concentration (5 mM IPTG), fluorescence intensities derived from the high-mCherry construct and the low-mCherry construct were approximately 50-fold and 5-fold higher when compared to the empty vector control, respectively (Fig. 1b). The results show that the constructed TFBs possess significantly different mCherry levels and both can clearly be distinguished from background fluorescence levels in liquid cultures using a microplate reader.

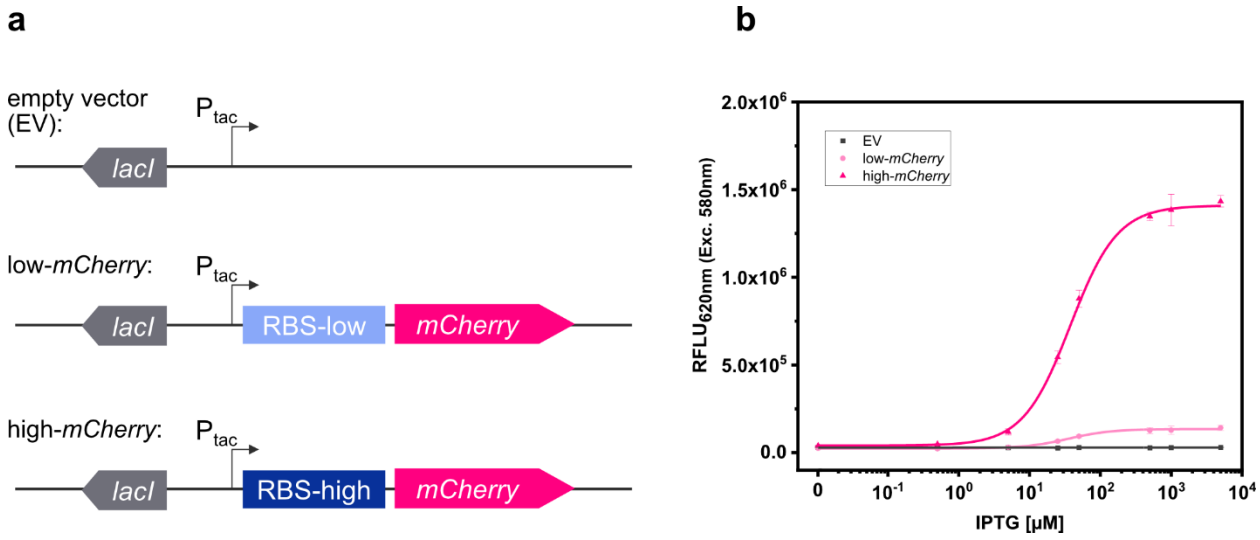

Figure 1: Schematic illustration of the genetic constructs for the expression platforms in pEKEx2 with different levels of mCherry translation initiation (**a**). Relative fluorescence units [RFLU] in presence of different IPTG concentrations after over-night cultivations in liquid media for *C. glutamicum* (pEKEx2) (EV: grey squares), *C. glutamicum* (pEKEx2_low_*mCherry*) (low-*mCherry*: light pink circles) and *C. glutamicum* (pEKEx2_high_*mCherry*) (high-*mCherry*: dark pink triangles) (**b**). A Hill function was fit to low-*mCherry* and high-*mCherry* data, and a linear fit was used for the empty vector (EV). Error bars represent standard deviation of four biological replicates.

To analyze the fluorescence signals derived from colonies of the three test strains *C. glutamicum* (pEKEx2), *C. glutamicum* (pEKEx2_low_*mCherry*), *and C. glutamicum* (pEKEx2_high_*mCherry*) via imaging, the strains were spotted on rectangular OmniTray (Singer Instruments, United Kingdom) agar plates supplemented with different IPTG concentrations (0 mM to 5mM). After 48 h of incubation, the mCherry fluorescence was analyzed in a fluorescence filter equipped FUSION FX (Vilber) imaging system. In presence of 5 mM IPTG, colonies carrying the reporter pEKEx2_high_*mCherry* revealed significantly

higher fluorescence intensities (mean value 8.09 x 10^2 ± 49 RFLU) when compared to colonies carrying the empty vector control (5.10 x 10^2 ± 43 RFLU) (Figure 2a, b). In contrast, statistical analysis via ANOVA revealed that fluorescence signals derived from colonies of *C. glutamicum* (*pEKEx2_low_mCherry*) (4.92 x 10^2 ± 24 RFLU) are not significantly different when compared to the empty vector control (Figure 2b). To note, increased exposure times (increased from 800 ms to 1000 ms) resulted in higher fluorescence levels for both the empty vector strain, the low-mCherry as well as high-mCherry variant (Fig. S1). Albeit, fluorescence signals obtained from the high-mCherry variant reached saturation at exposure times above 800 ms, the signals detected for the low-mCherry variant were still indistinguishable from signals obtained from the empty vector control strains under fully induced conditions (Fig. S1). Significant differences in the visual detection of biosensor fluorescence are a prerequisite towards rational decision-making during screens and the selection of variants. Thus, imaging is unlikely to be suitable for all biosensors and libraries [7].

The accurate positioning of 96-arrayed colonies on rectangular agar plates (in a 96-well scheme) was used to measure each colony with the optics of the plate reader. To confirm the accurate positioning of arrayed colonies, we performed an absorbance scan in a 96-well scheme with 30 x 30 scans per well for an OmniTray agar plate with 96- arrayed colonies in the plate reader (Fig. S2). The absorbance scan revealed that each colony, corresponding to the respective well, was centered irrespectively of the position of the individually measured colony (Fig. S2). The exact match of the positioning allowed the plate reader to perform single point measurements similar to measurements performed using 96-well plates. Accordingly, time required for analyses of the 96-colonies can be reduced from 90 minutes (scan mode) to 20 seconds (endpoint mode). Thus, the signals obtained from the colonies represent an average value from the colony rather than capturing heterogeneity across the colony.

Based on the precision and accuracy of the colony positions, the same agar plates used for fluorescence imaging were now analyzed using a standard microplate reader. Fluorescence analysis revealed that

179 signals detected via the plate reader for colonies equipped with the high-mCherry construct (average
180 fluorescence of $1.18 \times 10^{12} \pm 4.56 \times 10^{11}$ FLU), as well as for colonies with the low-mCherry construct
181 ($1.46 \times 10^{6} \pm 4.76 \times 10^{4}$FLU), were significantly different when compared to the empty vector control
182 ($3.23 \times 10^{5} \pm 1.70 \times 10^{4}$FLU) (Fig. 2c).

183 In addition, we tested the dose-dependent response of the TFB carrying strains
184 *C. glutamicum* (pEKEx2_low_mCherry and *C. glutamicum* (pEKEx2_high_mCherry) on agar plates with a
185 series of different IPTG concentrations (0 to 5 mM IPTG; Fig. 2d). Hereby, similar dose-response curves
186 were obtained for all strains when compared to the liquid cultures (Fig. 1b). As expected, no IPTG
187 dependent increase of mCherry fluorescence was detected for colonies of the empty vector control
188 strain *C. glutamicum* (pEKEx2). These results demonstrate that a microplate reader can be used for
189 assessing fluorescence signals in arrayed colonies.

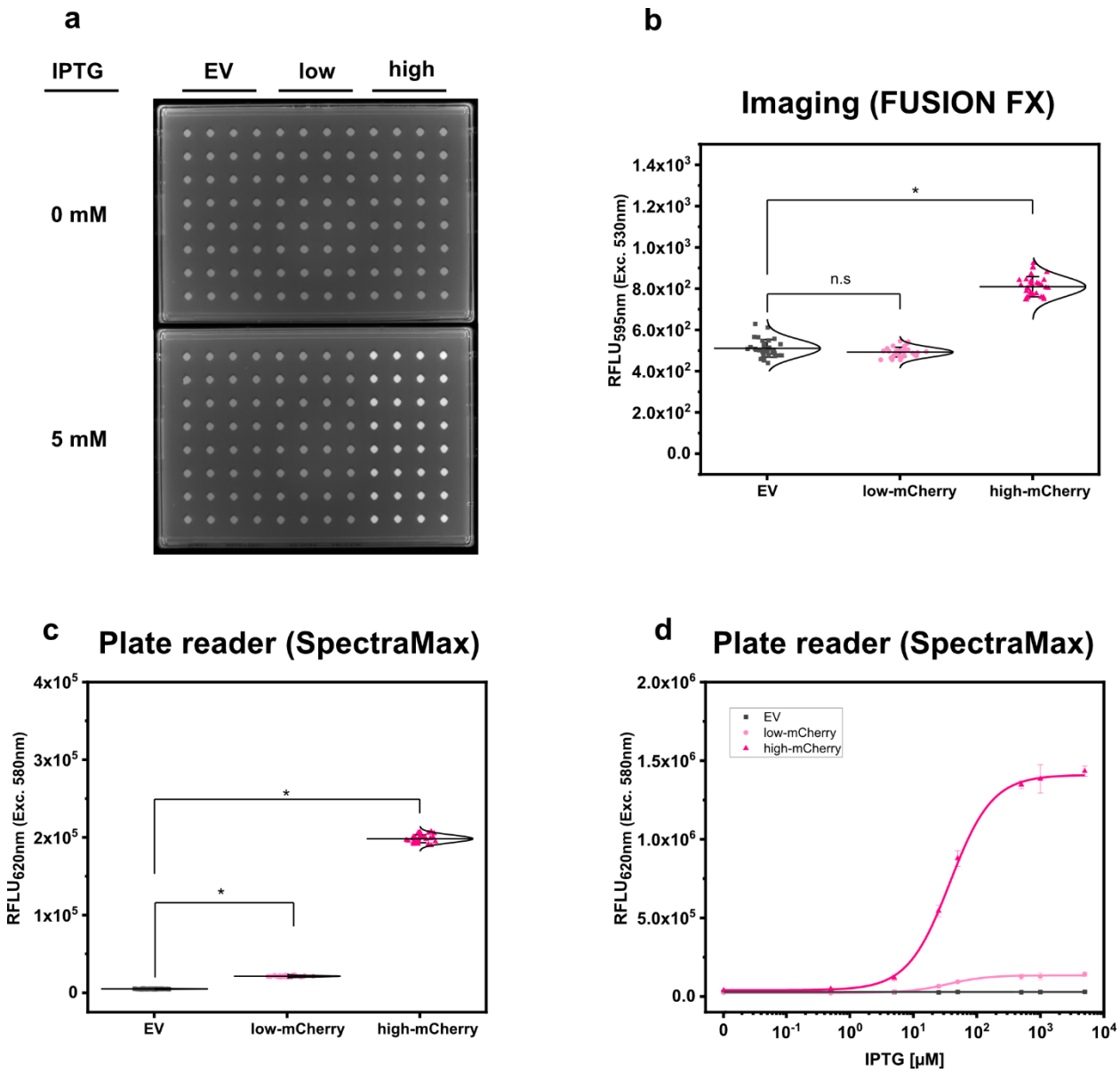

Figure 2: Comparison of fluorescence detection of arrayed bacterial colonies on agar plates via imaging and plate reader-based analysis. Representative fluorescence image of 32 colonies of *C. glutamicum* WT (pEKEx2) (EV: grey squares), *C. glutamicum* WT (pEKEx2_*low_mCherry*) (low: light pink circles) and *C. glutamicum* WT (pEKEx2_high_*mCherry*) (high: dark pink triangles) are spotted in absence (0 mM) or presence (5 mM) of IPTG by the use of the imaging system FUSION FX (Vilber) (**a**), the respective relative fluorescence units [RFLU] of determined for the different colonies (**b**) and the RFLU values of *C. glutamicum* colonies recorded via a plate reader (SpectraMax iD3 multi-mode plate reader (Molecular Devices LLC, U.S.A)) (**c**). RFLU values determined for arrayed colonies of *C. glutamicum* (pEKEx2) (EV: grey squares), *C. glutamicum* (pEKEx2_low_*mCherry*) (low-*mCherry*: light pink circles) and *C. glutamicum* (pEKEx2_high_*mCherry*) (high-*mCherry*: dark pink triangles) cultivated in presence of different IPTG concentrations (**d**). For sigmoidal curve fitting, Hill's equation (low-mCherry and high-mCherry). For the empty vector (EV), a linear fit was used. For fluorescence analysis using the plate reader excitation and emission were set to 580 nm and 620 nm, respectively. Imaging of arrayed colonies on agar plates was conducted using the imaging system FUSION FX (Vilber) equipped with a capsule for excitation (530 nm) and an emission filter (595 nm). Fluorescence signals were statistically analyzed with one-way-ANOVA followed by Tukey´s test ($^{n.s}$ $p > 0.05$; * $p \leq 0.001$). Error bars represent standard deviation of 32 colonies.

2.2 Microplate reader-based system for improved fluorescence analysis of promoter-based biosensors in *Saccharomyces cerevisiae* colonies on agar plates

We next addressed the applicability of the microplate reader-based method for the analysis of fluorescence signals from the broadly used fluorescent protein GFP in colonies of the well-known model-organism S. *cerevisiae.* For this purpose, two model strains of the haploid prototrophic yeast *S. cerevisiae* CEN.PK113-7D[23] were constructed by integration of expression cassettes with yeGFP as optical readout. Towards the development of reporter systems with different expression levels, a well-characterized weak constitutive promoter (PDA1) and strong glycolytic promoter (TDH3) were used to control varying levels of yeGFP production [24]. Prior to analyzing the fluorescence signals from *S. cerevisiae* (background control), *S. cerevisiae* (PDA1-yeGFP) (weak promoter), and *S. cerevisiae* (TDH3p-yeGFP) (strong promoter), strains were arrayed on OmniTray agar plates.

First, fluorescence analyses of GFP signals from arrayed *S. cerevisiae* colonies was performed using the microbial colony CCD imaging workstation Phenobooth (Singer Instruments), equipped with the manufacturer's filters for GFP fluorescence. As depicted in Fig. 3a, all colonies of *S. cerevisiae* (background) and *S. cerevisiae* (PDA1-yeGFP) (weak promoter) revealed fluorescence intensities at the same level. In contrast, significantly increased mean fluorescence intensities (1.28 ± 0.14 fold) were measured for colonies of *S. cerevisiae* (TDH3p-yeGFP) (strong promoter). However, individual signals from colonies equipped with the strong promoter still partly overlap with the values derived from the background control colonies. This means that during a random screen a high number of "GFP positive" strains would have remained undetected resulting in a low screening efficiency. Next, fluorescence signals were analyzed by the use of the imaging system FUSION FX (Vilber), equipped with a capsule and a filter for excitation at 435nm and emission at 480nm, respectively. The mean fluorescence signals derived from 96 colonies of *S. cerevisiae* (PDA1-yeGFP) (weak promoter) and *S. cerevisiae* (TDH3p-yeGFP) (strong promoter) were significantly increased by 1.30 ± 0.10 fold and 2.37 ± 0.22 fold when

compared to the background control, respectively (Fig. 3b). Even though not all individual colonies of *S. cerevisiae* (PDA1-yeGFP) can explicitly be distinguished from colonies of the control *S. cerevisiae* strain, which shows background levels of fluorescence, fluorescence analysis via the FUSION FX imaging system has significantly been improved when compared to the use of an imaging workstation (Phenobooth, Singer Instruments).

As a next step, the microplate reader-based method was used to analyze yeGFP signals derived from the different promoters in *S. cerevisiae*. As described for mCherry signals in *C. glutamicum* by the use of the microplate reader SpectraMax, an average value of $6.62 \times 10^4 \pm 8.59 \times 10^3$ RFLU, $1.19 \times 10^5 \pm 1.22 \times 10^4$ RFLU and $7.46 \times 10^5 \pm 8.74 \times 10^4$ RFLU was determined for *S. cerevisiae* (background), *S. cerevisiae* (PDA1-yeGFP) (weak promoter) and *S. cerevisiae* (TDH3p-yeGFP) (strong promoter), respectively (Fig. 3c). This corresponds to a significant 1.80 ± 0.16 fold (weak promoter) and 11.30 ± 1.02 fold (strong promoter) increase when compared to the background control. In contrast to fluorescence imaging, all individual signals obtained for the 96 analyzed colonies harboring both the weak promoter (PDA1-yeGFP) or the strong promoter (TDH3p-yeGFP) possessed higher fluorescence levels when compared to background control colonies (Fig. 3c).

To demonstrate transferability of the microplate reader-based approach, we next analyzed fluorescence signals in arrayed colonies using a CLARIOstar^{Plus} as a different plate reader device. When compared to *S. cerevisiae*, the mean fluorescence intensity measured for all colonies equipped with the weak promoter (PDA1-yeGFP) and strong promoter (TDH3p-yeGFP) were increased 1.93 ± 0.13 fold and 12.36 ± 0.89 fold, respectively (Fig. 3d). These results are in accordance with results obtained via the SpectraMax plate reader.

Taken together, microplate reader-based analysis of colony fluorescence enables the precise and sensitive detection of fluorescence levels of reporter proteins in various microorganisms. To facilitate

fluorescence analysis via this approach it is required that the colonies are arrayed in a microtiter-based format. If it is not possible to array the microbial colonies, fluorescence analysis via sensitive imaging systems equipped with adequate sets of filters, such as those used here for the FUSION FX (Vilber) imaging system, are a good alternative, although their incorporation in highly automated workflows is a challenge.

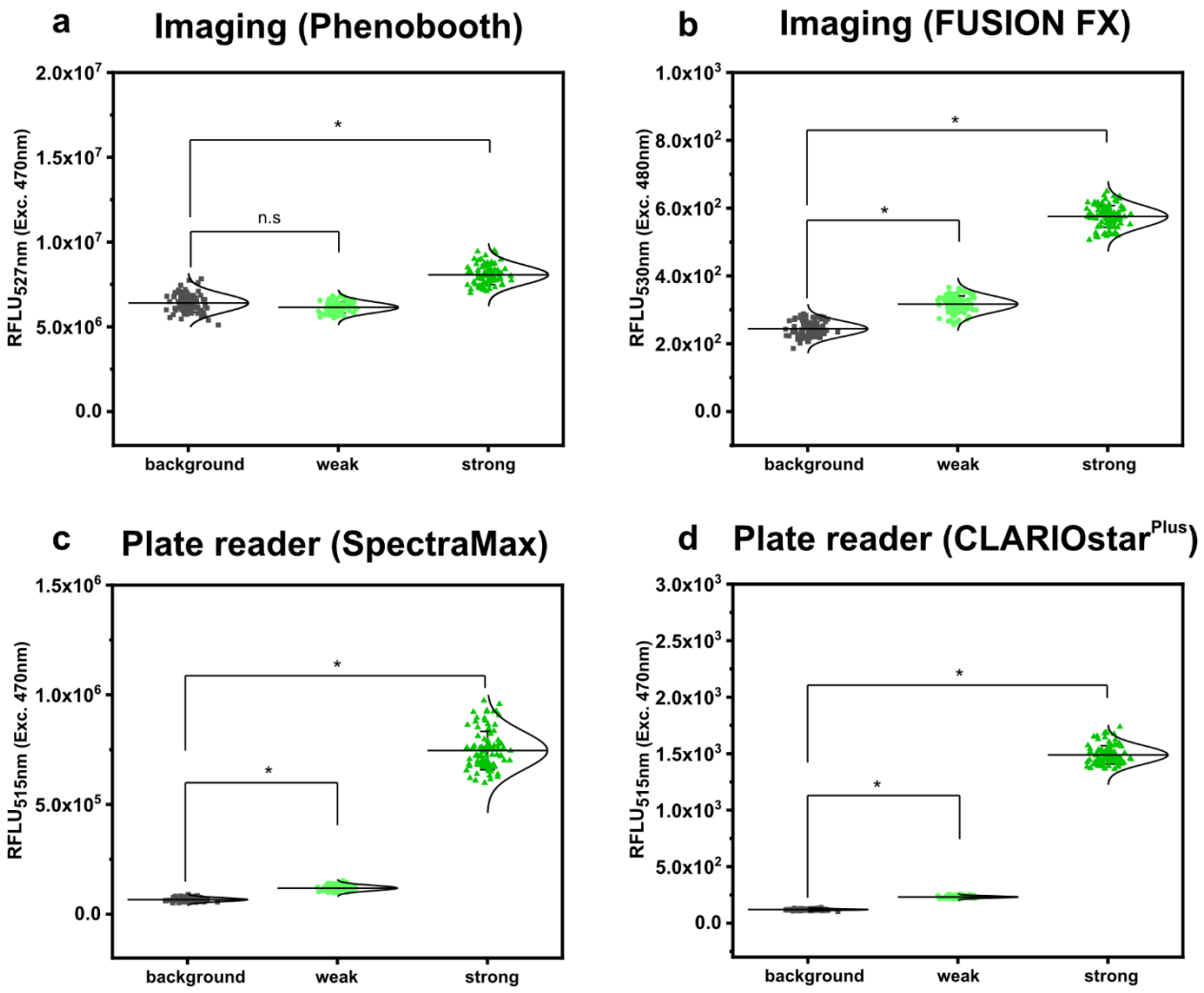

Figure 3: Comparison of fluorescence detection of arrayed *Saccharomyces cerevisiae* colonies on agar plates via imaging and plate reader-based analysis. Relative fluorescence units (RFLU) of 96-arrayed colonies of *Saccharomyces cerevisiae* (background; grey squares), *Saccharomyces cerevisiae* (TDH3p-yeGFP) (weak; light green circles) and *Saccharomyces cerevisiae* (PDA1p-yeGFP) (strong, green triangles) analyzed via imaging using the Phenobooth (**a**) or the FUSION FX (Vilber) (**b**). Further, fluorescence analysis was performed using the plate reader devices SpectraMax (**c**) and CLARIOstar^{Plus} (**d**). RFLU were obtained by normalizing the fluorescence intensity to the colony size (perimeter). Fluorescence signals were statistically analyzed with one-way-ANOVA followed by Tukey´s test ($^{n.s}$ $p > 0.05$; * $p \leq 0.001$). Mean values from 96- replicates are shown (solid horizontal line).

2.3 Microplate reader-based analysis of the pH-sensitive protein mCherryEA improves accuracy of internal pH measurements in *E. coli* colonies

The use of a monochromator equipped microplate reader allowed us to set optimal excitation and emission wavelength settings for the sensitive detection of mCherry and GFP signals from microbial colonies. To test if the versatility and precision of the wavelength settings via the monochromators also enables sensitive analyses of fluorescence signals from ratiometric fluorescent reporter proteins, we aimed to compare analysis of fluorescence signals from the internal pH-sensor protein mCherryEA in arrayed *E. coli* colonies via a plate reader to the recently described approach via fluorescence imaging in a FUSION FX (Vilber) imaging system[8].

For this purpose, colonies of the strain *E. coli* MG1655 (pXMJ19_*mCherryEA*) and the empty vector control strain *E. coli* MG1655 (pXMJ19) were arrayed on SB agar plates (pH 7.0). After cultivation, 5 µL of PBS buffer supplemented with 0.05 % CTAB and with set pH values between 7.0 and 8.5 were applied onto the colonies, as recently described [8]. At this CTAB concentration the *E. coli* cell membrane is permeabilized allowing the internal pH to become adjusted to the set external pH [17]. The fluorescence of the colonies was analyzed using an excitation scan (400 nm – 590 nm) at an emission wavelength of 630 nm and using the positions of the 96-well measurement mode of the plate reader. As depicted in Fig. 4a, two excitation maxima at 454 nm and 580 nm were obtained for colonies of *E. coli* MG1655 (pXMJ19_*mCherryEA*), which are in accordance to the maxima observed in recently performed excitation scans of bacterial strains harboring the pH- sensitive mCherryEA protein in liquid culture[8,25]. As expected, no characteristic mCherryEA sensor signal was measured for the empty vector control *E. coli* MG1655 (pXMJ19) (Fig. 4a). When applying PBS buffer (+ CTAB) with a set pH of 7.0 to the colonies, an emission intensity of 5.8E + 06 FLU was measured at 454 nm excitation, whereas the signal obtained upon an excitation at 580 nm was higher with 6.8E + 06 FLU (Fig. 4a); when a PBS buffer (+ CTAB) with a higher pH (8.5) was applied to a colony, the fluorescence intensity obtained for an

291 excitation at 454 nm increased (8.3E + 06 FLU) and decreased at an excitation at 580 nm (4.4E + 06 FLU).
292 This pH-dependent response of the signals for mCherryEA at the two excitation wavelengths indicates
293 that the ratiometric response of the biosensor protein mCherryEA in *E. coli* colonies on agar plates can
294 be measured using the microplate reader-based system. Further, fluorescence from *E. coli* MG1655
295 (pXMJ19_*mCherryEA*) colonies treated with PBS buffer (+ CTAB) with set pH values ranging from 7.0 to
296 8.5 (Fig. 4b) were analyzed using the plate reader (Exc. 454 nm/ 580 nm) and the recently established
297 imaging method (Exc. 440 nm/ Exc. 530 nm) [8]. The biosensor ratios determined for the imaging method
298 increased linear from 0.62 ± 0.02 (pH 7.0) to 1.08 ± 0.03 (pH 8.5) upon increasing the pH (Fig. 4b). A
299 similar biosensor response was detected with the microplate reader-based method, resulting in an
300 increase from 0.85 ± 0.03 (pH 7.0) to 1.35 ± 0.03 (pH 8.5) (Fig. 4b).

301 Next, 120 colonies arrayed on a rectangular agar plate were analyzed *via* the two different methods
302 (imaging and plate reader) and the internal pH for each colony determined and visualized with a heat
303 map, where each square corresponds to a single colony (Fig. 4c). For both methods, the mean internal
304 pH obtained by the imaging method and the plate reader method was similar with 7.66 ± 0.13 and 7.65
305 ± 0.03, respectively (Fig. 4d). This agrees with the reported cytoplasmic pH of *E. coli* which is normally
306 maintained within the range of 7.4-7.9[26–28] and recently determined internal pH levels in *E. coli* MG1655
307 colonies on agar plates under similar conditions[8]. However, differences with respect to the distribution
308 of the determined internal pH values were observed when comparing the data obtained for the two
309 different methods (Fig. 4d). The plate reader method established here allowed us to narrow down the
310 distribution from 7.26-7.82 (ΔpH= 0.56; imaging method) to 7.59-7.76 (ΔpH= 0.17; plate reader
311 method), corresponding to a reduction of 0.39 pH units. As the pH is logarithmically and inversely
312 related to the concentrations of hydrogen ions in a solution, the accuracy of the analysis is improved by
313 390 %. The broader distribution obtained by the imaging method might be caused by reflection artefacts
314 from the transparent edges of the OmniTray plates. To note, the imaging method relies on a one-step

315 excitation of the whole plate, whereas measurements performed in the microplate reader allowed us to
316 measure colonies individually, similar to measurements performed in a 96-well microplate. Moreover,
317 the microplate reader-based method allows operators to set excitation and emission wavelengths on
318 demand and thus perfectly matches the two excitation maxima displayed by the sensor protein
319 mCherryEA. In contrast, the imaging system FUSION FX (Vilber) needs to be equipped with the most
320 suited capsules and filters available (Exc. 440 nm & Exc. 530 nm), which often do not match the
321 properties of the fluorescent protein[25,29,30].

322

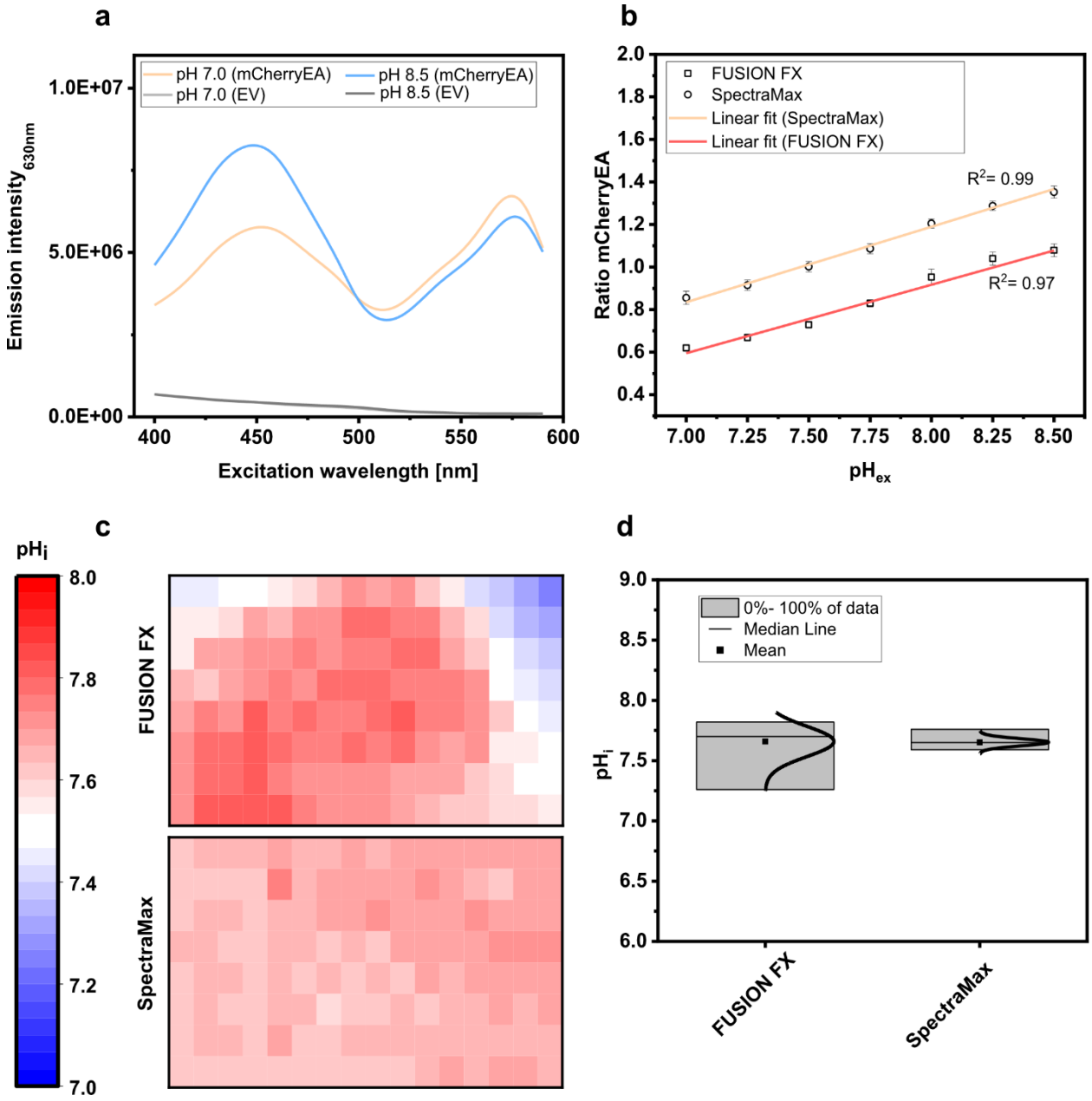

Figure 4: Excitation scan (400 nm – 590 nm) recording the emission intensity at 630 nm in colonies of *E. coli* MG1655 (pXMJ19_*mCherryEA*) (mCherryEA) and the empty vector control strain *E. coli* MG1655 (pXMJ19) (EV) after applying 5 µL PBS buffer supplemented with cetyltrimethylammonium bromide (CTAB; final concentration 0.05 % (w/v)) with a set pH of 7.0 and 8.5 (**a**) and ratiometric biosensor signals obtained by dividing the emission intensity at 454 nm by 580 nm upon applying PBS buffer with pH values ranging from 7.0 – 8.5 (**b**). Calculation of the internal pH for biosensor signals recorded from 120 colonies either *via* imaging using the FUSION FX imaging system equipped with two capsules (Exc. 440 nm & Exc. 530 nm) and one emission filter (Em. 595 nm) as recently described in Hartmann et al. 2022[8] or with a microplate reader system (SpectraMax) (**c**) and data distribution with median and mean values obtained by the two different approaches (**d**). Error bars represent standard deviation from at least three replicates.

2.4 Mycothiol is required to maintain a reduced environment in *C. glutamicum* colonies growing on agar plates

The improved accuracy using the plate reader-based biosensor analysis represents a significant step forward with respect to screening approaches requiring high sensitivities. Moreover, the high flexibility brought by the monochromatic technology of the plate reader device easily adapts to other fluorescent reporter proteins without causing additional costs and effort to equip imaging devices with appropriate filters. Thus, we next tested this novel technique by applying a ratiometric redox biosensor protein called Mrx1-roGFP2 in *C. glutamicum* colonies.

The abundant low molecular weight (LMW) mycothiol (MSH) functions to maintain the reduced state of the cytoplasm and represents the main non-enzymatic antioxidant in high-GC Gram-positive bacteria, such as the industrial amino acid producer *C. glutamicum* [31–33]. Recently, the genetically encoded redox biosensor protein Mrx1-roGFP2 was successfully applied in *C. glutamicum* WT and the MSH-deficient mutant strain *C. glutamicum* Δ*mshC* to monitor dynamic redox changes in liquid cultures[16,34]. Mutant strains lacking MSH have revealed high susceptibility towards oxidative stress resulting in an impaired growth behavior when cells were exposed to artificial oxidants in shaker-flasks[32]. In absence of artificial oxidants, growth of the MSH-deficient mutant strain proceeded similar to the wild type strain[16,32,34], even though biosensor measurements in the mutant strain revealed an oxidative redox shift [16,34]. Detecting intracellular changes (i.e. oxidative stress) prior to the occurrence of a growth defect is an important advance for the development of highly sensitive sensor-based screening approaches. This prompted us to test the analysis of intracellular redox states in arrayed colonies of *C. glutamicum* WT and a mutant strain lacking MSH using the redox biosensor protein Mrx1-roGFP2.

To analyze the redox states in *C. glutamicum* colonies, the 380 nm/470 nm biosensor ratios from 120 arrayed colonies of WT_Mrx1- roGFP2 and the MSH-deficient mutant strain Δ*mshC*_Mrx1-roGFP2 were

358 determined. The Mrx1-roGFP2 biosensor consists of redox sensitive GFP2 (roGFP2) which harbors two
359 Cys residues. Upon oxidation it forms a disulfide bond, resulting in an increase of the respective
360 biosensor ratio (Exc. 380 nm/ Exc. 470 nm), whereas it responds in the opposite way upon reduction of
361 the biosensor protein. As depicted in Fig. 5a, the mean values of the biosensor ratios were significantly
362 different with 0.82 ± 0.01 and 1.52 ± 0.02 for WT_Mrx1-roGFP2 and Δ*mshC*_Mrx1-roGFP2, respectively,
363 indicating a more oxidized state of the biosensor protein Mrx1-roGFP2 in the Δ*mshC*_Mrx1-roGFP2
364 strain background on agar plates (Fig. 5a). This is in accordance to previous measurements conducted in
365 liquid cultures with biosensor ratios of 1.0 ± 0.02 (WT_Mrx1-roGFP2) and 1.52 ± 0.03 (Δ*mshC*_Mrx1-
366 roGFP2)[16].

367 Further, we validated the dynamic response and functionality of the sensor protein Mrx1-roGFP2 in
368 colonies by applying Dithiothreitol (DTT; 100 mM) and Natriumhypochlorite (NaOCl; 100 mM) as
369 reducing and oxidizing agents, respectively. For this, 5 µL drops were applied onto WT_Mrx1-roGFP2
370 and Δ*mshC*_Mrx1-roGFP2 colonies followed by real-time monitoring of the biosensor signals. Prior to
371 the colony treatment, WT_Mrx1-roGFP2 was maintaining stable biosensor ratios between 0.76 - 0.78
372 followed by a strong reduction or increase of the biosensor ratio upon applying DTT or NaOCl,
373 respectively (Fig. 5b). After five minutes of incubation, fully reduced (DTT; biosensor ratio of 0.53) and
374 fully oxidized (NaOCl; biosensor ratio of 1.4) biosensor ratios were recorded until the end of the
375 experiment (Fig. 5b). The treatment with PBS only temporarily induced a slight decrease of the recorded
376 biosensor ratio but then was restored to initially recorded biosensor ratios (Fig. 5b). In contrast,
377 Δ*mshC*_Mrx1-roGFP2 colonies revealed biosensor ratios between 1.4 - 1.45 prior to the treatment of the
378 colonies. The addition of DTT buffer solution resulted in a strong reduction of the biosensor ratio
379 reaching fully reduced ratios of 0.54, six to eight minutes following the treatment (Fig. 5c). As expected,
380 treatment with NaOCl just slightly increased the ratio to 1.54 due to its almost fully oxidized state, when
381 compared to a final biosensor ratio of 1.4 for colonies treated with PBS buffer only (Fig. 5c). To note, no

382 alteration of the recorded fluorescence signals was observed when performing the same experiment
383 using the *C. glutamicum* WT controls strain, indicating that the measured change of the ratiometric
384 biosensor signals in both sensor strains can be attributed to the biosensor protein Mrx1-roGFP2 (Fig.
385 S3).

386 Based on the measured biosensor ratios, the oxidation degree (OxD) of the biosensor protein Mrx1-
387 roGFP2 was calculated according to equation 1. OxD values of 0.93 ± 0.03 and 0.33 ± 0.03 were
388 calculated for the Mrx1-roGFP2 biosensor in Δ*mshC*_Mrx1-roGFP2 and WT_Mrx1-roGFP2 colonies on
389 agar plates, respectively (Fig. 5d). The results are consistent with previous studies performed in shaker-
390 flasks under non-stressed conditions where OxD values between 0.3 - 0.5 were reported for WT_Mrx1-
391 roGFP2[16,34]. In contrast, almost fully oxidized biosensor states were reported for the MSH-deficient
392 mutant strain (OxD = 0.8 - 0.95)[16,34]. Upon the formation of ROS, the redox-active sulfhydryl group of
393 MSH can either scavenge free radicals directly or functions as a cofactor for antioxidant enzymes
394 resulting in formation of oxidized mycothiol disulfide (MSSM)[31,35–38]. Accordingly, the lack of MSH
395 elevates the intracellular ROS levels and in turn induces an auto-oxidation of the biosensor protein
396 Mrx1- roGFP2 in Δ*mshC*_Mrx1-roGFP2. Thus, previous results and the results of this study indicate the
397 major role of MSH for the overall redox homeostasis under aerobic growth conditions in shake-flasks
398 cultivations but also in colonies growing on agar plates.

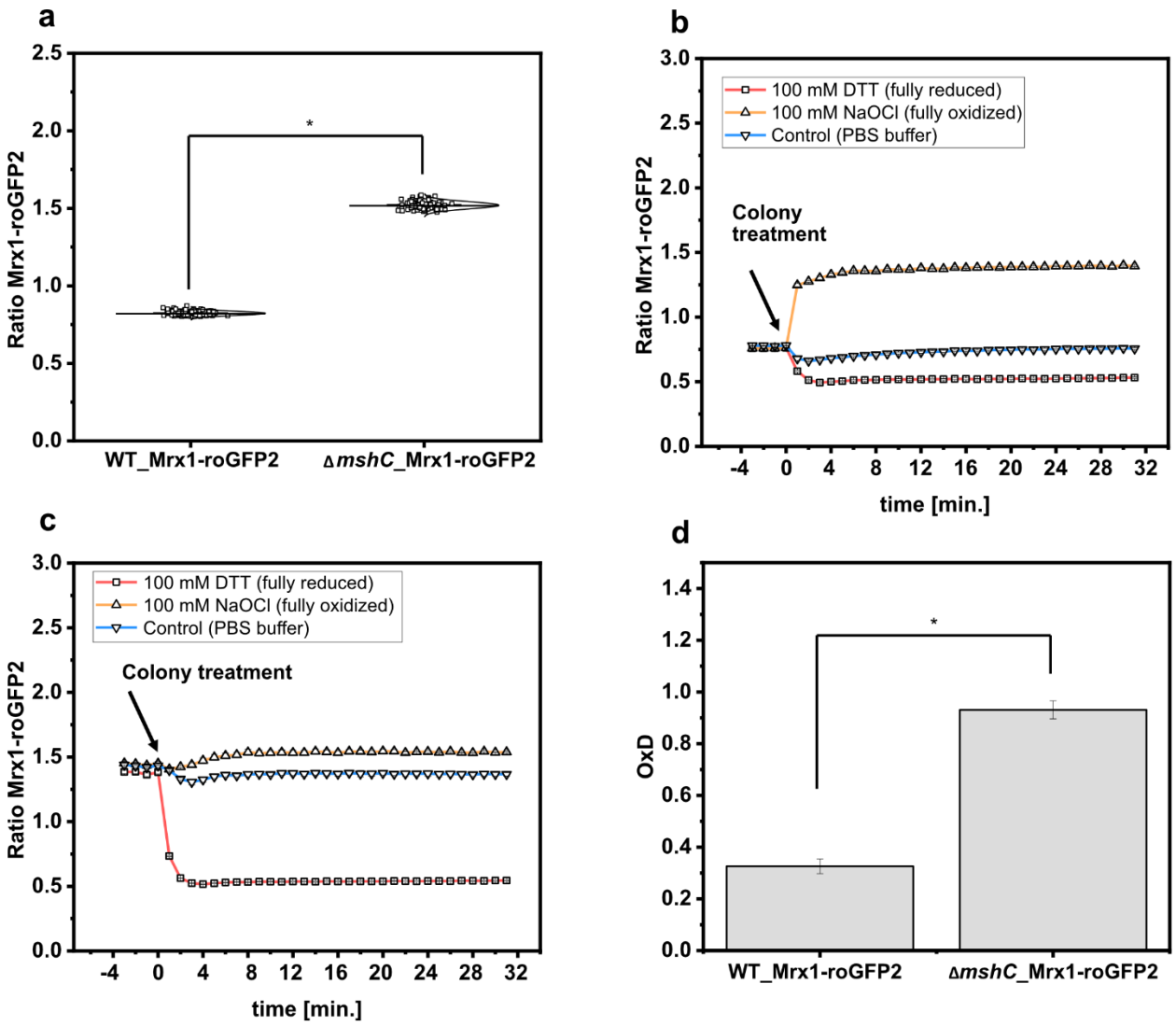

Figure 5: Calculated biosensor ratio (Exc. 380nm/ Exc. 470 nm) of the sensor protein Mrx1-roGFP2 in colonies of *C. glutamicum* WT_Mrx1-roGFP2 (WT_Mrx1-roGFP2) and *C. glutamicum* Δ*mshC*_Mrx1-roGFP2 (Δ*mshC*_Mrx1-roGFP2) (**a**) and real-time monitoring of the response of the ratiometric signal of the biosensor Mrx1-roGFP2 upon applying DTT (100 mM) (reducing agent), hypochlorite (100 mM) (oxidizing agent) and PBS buffer (control) onto WT_Mrx1-roGFP2 (**b**) and Δ*mshC*_Mrx1-roGFP2 colonies (**c**). Calculation of the oxidation degree (OxD) by normalizing biosensor ratios to fully oxidized and reduced states (**d**). For sensor analysis, 30 colonies from four independent agar plates and experiments were analyzed for each strain (120 colonies in total). Biosensor ratios were analyzed with one-way-ANOVA followed by Tukey´s test ($^{n.s}$ $p > 0.05$; * $p \leq 0.001$).

2.5 Ratiometric biosensor signals are independent of the colony size

Fluorescence signals derived from single fluorescent proteins need to be normalized to the OD_{600} (96-well screen) or colony size (agar screen). In contrast to single fluorescent proteins, a ratiometric fluorescent protein can be normalized to the second fluorescence signal rather than growth related parameters. This implies that a ratiometric biosensor signal should not be affected by changes of the colony size during screens on agar plates.

To test this, a dilution series (different set OD_{600}) of *C. glutamicum* WT (WT), *C. glutamicum* WT_Mrx1-roGFP2 (WT_Mrx1-roGFP2) and *C. glutamicum* Δ*mshC*_Mrx1-roGFP2 (Δ*mshC*_Mrx1-roGFP2) was spotted on rectangular OmniTray plates with solidified CGXII minimal medium (1 % Glucose) (Fig. 6a). After 48 hours of incubation, the final colony size was determined for all spotted dilutions and the size reduction calculated relative to the highest applied OD_{600} (Fig. 6a). For the highest applied OD_{600} (10^{1}), defined as 100 % colony size, the area was determined to be 680 ± 29, 610 ± 52 and 590 ± 49 pixels for the WT, WT_Mrx1-roGFP2 and the Δ*mshC*_Mrx1-roGFP2 colonies, respectively (Fig. 6a). Upon applying higher dilutions (stepwise 1:10), the relative colony size was reduced by approximately 10 % for each dilution step and a relative colony size of 55 ± 8 %, 61 ± 2% and 54 ± 0.4 % was reached upon applying an OD_{600} of 10^{-3} for the WT, WT_Mrx1-roGFP2 and Δ*mshC*_Mrx1-roGFP2 strain, respectively (Fig. 6a). For this dilution, the circular morphology of the colonies was impaired leading to inaccuracies with respect to the colony size determination for further dilutions (Fig. 6a). Next, the positions of the arrayed colonies from the dilution series were selected and the fluorescence intensity derived from the sensor protein Mrx1-roGFP2 analyzed. Absolute fluorescence intensities measured at 510 nm (Exc. 470 nm) revealed increased fluorescence levels in colonies of WT_Mrx1-roGFP2 (5.4×10^{6} – 1.3×10^{7} FLU) and Δ*mshC*_Mrx1-roGFP2 (4.2×10^{6} – 1.03×10^{7} FLU) strains when compared to the parental wild type strain *C. glutamicum* (1.90 – 3.90×10^{6} FLU) (Fig. 6b). Absolute fluorescence intensities decreased upon a reduction of the colony size (Fig. 6b). In accordance with the fluorescence analysis for mCherry or GFP in

436 the previous sections, relative fluorescence intensities were calculated by normalizing the absolute
437 fluorescence intensity to the perimeter of the colony. As expected, fluorescence signals normalized to
438 the measured perimeter of the colonies resulted in stable relative fluorescence intensities until a colony
439 size reduction of 70 % was reached (Fig. S4). Next, the second fluorescence signal (Exc.
440 380 nm/Em. 510 nm) was measured for all colonies and the biosensor ratio calculated (Exc. 380 nm/ Exc.
441 470 nm). The ratiometric biosensor signal independently of the colony size, remained stable between
442 1.0 – 1.1 and 1.4 – 1.5 in WT_Mrx1-roGFP2 and Δ*mshC*_Mrx1-roGFP2 colonies, respectively (Fig. 6c). As
443 discussed in the previous section, higher biosensor ratios measured for the MSH-deficient strain are
444 caused by the more oxidized state of the biosensor protein Mrx1-roGFP in this strain background. To
445 note, increased ratiometric signals (between 2.5 to 4.0) for the agar surface (no colony) and for
446 *C. glutamicum* not harboring the biosensor protein Mrx1-roGFP2 are due to low background
447 fluorescence at 510 nm (Exc. 470 nm) but a higher background fluorescence at 510 nm when excited at
448 380 nm (Fig. 6c).

449 Taken together, the results demonstrate that the signal derived from a ratiometric biosensor is robust
450 against variations of colony size and the morphology of colonies (Fig. 6c). This makes ratiometric FRPs a
451 powerful tool when conducting screens of mutant libraries comprising different phenotypes (e.g. growth
452 behavior). Furthermore, agar plate-based screens provide the advantage that the tested strains can be
453 exposed to various conditions at the same time (replica plating) [19,39]. Conducting screens under
454 industrially relevant conditions (e.g. pH gradients) supported by the use of ratiometric "stress"
455 biosensors will facilitate the development of structured metabolic models for industrially relevant
456 organisms. This bridges metabolic engineering and bioprocess development allowing for the
457 development of computational models suitable for both cell factory design and process optimization at
458 industrial scales in the future [40].

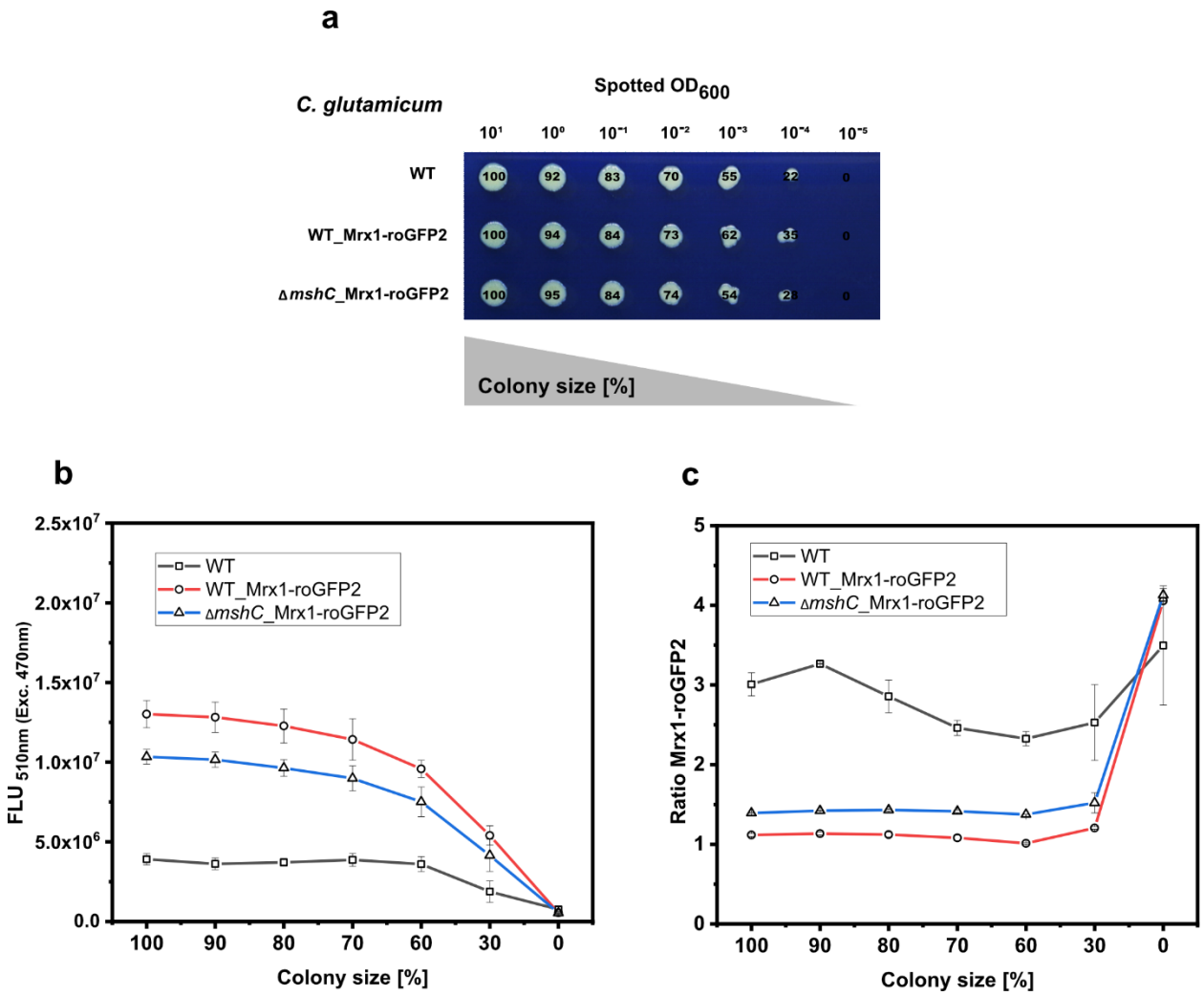

Figure 6: Robotic spotting of a dilution series of *C. glutamicum* WT (WT), *C. glutamicum* WT_Mrx1-roGFP2 (WT_Mrx1-roGFP2) and *C. glutamicum* Δ*mshC*_Mrx1-roGFP2 (Δ*mshC*_Mrx1-roGFP2) liquid cultures with different set optical densities measured at 600 nm (OD_{600}) and determination of the colony size relative to the highest spotted OD_{600} (**a**). Absolute fluorescence intensities measured at 510 nm (Exc. 470 nm) to validate the presence of Mrx1- roGFP2 in WT_Mrx1-roGFP2 and Δ*mshC*_Mrx1-roGFP2 colonies (**b**), and the ratiometric biosensor signal of Mrx1-roGFP2 in the different colonies (**c**). Robotic spotting was performed using a replica plating Robot ROTOR. Dilution series was grown on OmniTray plates with CGXII media supplemented with 1% Glucose. Fluorescence analysis of the colonies from the dilution series was performed in a microplate reader (SpectraMax iD3). For the calculation of the ratiometric biosensor signal, the emission intensity at 510 nm was recorded upon an excitation at 380 nm and 470 nm and the former was divided by the latter (Exc. 380 nm/ Exc. 470 nm). Mean values from two independent experiments are shown.

3 Conclusion

Phenotypic screenings using arrayed colonies is a widely applied approach to screen strain libraries for particular variants with desired phenotypes. Genetically encoded biosensors are powerful analytical tools to support the rational decision making for strain selection as intracellular states can easily be assessed in a high-throughput manner. However, imaging analysis often limits the applicability of biosensors as the optical set-up of the utilized imaging device does not match with the properties of the fluorescent protein. The microplate reader-based system for sensor analysis established here provides the advantage of a monochromatic technology, which provides high flexibility with respect to different excitation and emission wavelengths. This novel technique has revealed high sensitivity for the detection of low fluorescence levels making it attractive for the development and optimization of genetic circuits regulating harmful targets. In addition, the monochromatic technology enables great opportunities to utilize FRPs, which application to date is often limited due to their complex ratiometric fluorescent properties. The ratiometric readout makes these types of biosensors highly robust against signal fluctuations caused by the colony size or morphology of the colony. Moreover, applications of such biosensors enables the measurement of complex intracellular states such as oxidative stress or the internal pH in real- time due to their fast dynamics. The microplate reader-based analysis established here can easily be adapted to further biosensors and combinations thereof without causing additional costs and effort to install adequate filter modules. Thus, this technique is expected to provide new possibilities for comprehensive phenotypic screenings and novel applications in metabolic engineering and systems biology.

4 Materials and methods

Strains, media, and culture conditions

Bacterial strains, yeast strains, and plasmids used in this study are listed in Table 1. Cloning was carried out using *E. coli* DH5 α, cultivated in Lysogeny Broth (LB) medium[41]. *C. glutamicum* was cultivated using BHI- media (Sigma Aldrich, Germany). *E. coli* MG1655 was cultivated in SB- medium (5 g/L yeast extract; 10 g/L BactoTryptone; 100 mM NaCL; 50 mM KCl, buffered with 50 mM TRIS; pH 7.0) as recently described[8]. For preparation of agar plates, 16 g/L agar was added to the respective media. Strains carrying plasmids were cultivated in presence of kanamycin (50 µg/mL) or chloramphenicol (20 µg/mL). If required and unless stated otherwise, 1 mM IPTG was added to induce gene expression.

Table 1: Bacterial strains, yeast strains and plasmids used in this study.

Bacterial Strains/ Plasmids	**Description**	**Reference/ Resource**
Escherichia coli		
E. coli DH5 α	F-ϕ80dlacZ Δ(lacZYA-argF) U169 deoRsupE44ΔlacU169 (f80lacZDM15) hsdR17 recA1 endA1 (rk- mk+) supE44gyrA96 thi-1 gyrA69 relA1	[42]
E. coli MG 1655	F^- lambda- ilvG-rfb-50rpH-1	[43]
E. coli MG 1655 (pXMJ19)	*E. coli* MG 1655 carrying the vector pXMJ19	[8]
E. coli MG1655 (pXMJ19_*mCherryEA*)	*E. coli* MG 1655 carrying a derivative of pXMJ19 for IPTG-inducible *mCherryEA* expression	[8]
***Corynebacterium glutamicum* ATCC 13032**	**Wild type**	[44]
C. glutamicum (pEKEx2)	*C. glutamicum* WT carrying the shuttle vector pEKEx2	This study
C. glutamicum (pEKEx2_low_*mCherry*)	*C. glutamicum* WT carrying a derivative of the shuttle vector pEKEx2 for IPTG inducible expression of the *mCherry* gene	This study
C. glutamicum (pEKEx2_high_*mCherry*)	*C. glutamicum* WT carrying a derivative of the shuttle vector pEKEx2 for IPTG inducible expression of the *mCherry* gene	This study
C. glutamicum WT_Mrx1-roGFP2	*C. glutamicum* WT with integrated P_{tuf}-*mrx1-roGFP2*	[34]

	into the intergenic region of *cg1121-cg1122*	
C. glutamicum Δ*mshC* _Mrx1-roGFP2	*C. glutamicum* WT deletion of *mshC* and integrated P_{tuf}-*mrx1-roGFP2* into the intergenic region of *cg1121-cg1122*	[34]
S. cerevisiae **CEN.PK113-7D**	**Wild type**	[23]
*S. cerevisiae (*TDH3p-yeGFP_XII-1)	*S. cerevisiae with integrated TDH3p-yeGFP-CYC1t and NatMX resistance cassette into the intergenic integration site XII-1*	This study
*S. cerevisiae (*PDA1p-yeGFP_XII-1)	*S. cerevisiae with integrated PDA1p-yeGFP-CYC1t and NatMX resistance cassette into the intergenic integration site XII-1*	This study
Plasmids		
pEKEx2	Expression vector; p*tac lacI*^{q} Km^r	[45]
pXMJ19	Expression vector; p*tac lacI*^{q} Cam^r	[46]
pEKEx2_low_*mCherry*	pEKEx2 derivative for IPTG-inducible *mCherry* gene expression. Upstream of *mCherry* a weak RBS was inserted.	This study
pEKEx2_high_*mCherry*	pEKEx2 derivative for IPTG-inducible *mCherry* gene expression. Upstream of *mCherry* a high RBS including a spacer of 6 nt was inserted. This RBS-spacer combination was reported as strong RBS by Shi et al. 2018.[47]	This study
pXMJ19_*mCherryEA*	pXMJ19 derivative for IPTG-inducible *mCherryEA* gene expression	[8]
pCfB2197	EasyClone system-based yeast integrative vector carrying loxP-flanked natMX marker, integration into *S. cerevisiae* XII-1 chromosomal location, USER site for cloning amp resistance.	[48]
pLK0106	pCfB2197 containing yeGFP gene under control of PDA1 promoter.	This study
pLK0107	pCfB2197 containing yeGFP gene under control of TDH3 promoter.	This study

Strain construction

The two plasmids pEKEx2_low_*mCherry* and pEKEx2_high_*mCherry* were assembled *via* Gibson cloning using the Gibson Assembly® Master Mix (NEB, USA) according to the manufacturer's instructions. For his purpose pEKEx2 was first linearized using SacI (NEB, USA). The gene for mCherry was amplified by PCR using the primer pairs low_*mCherry*_fw and low_mCherry_rev (Table S1) or high_*mCherry*_fw and high_*mCherry*_rev for pEKEx2_low_*mCherry* and pEKEx2_high_*mCherry*, respectively. All plasmids were introduced into competent *E. coli* DH5α and analyzed via sequencing prior to further use. Transformation of electrocompetent *C. glutamicum* cells and strain validation were performed as described previously[49].

To construct the two plasmids pLK0106 and pLK0107 for yeast, DNA fragments constituting the weak PDA1 promoter or the strong TDH3 promoter [24] and the yeGFP open reading frame [50] were synthesized as double-stranded gene fragments (Twist Bioscience). The integrative vector pCfB2197 from the EasyClone 2.0 toolkit was used for plasmid construction, which allowed for selection in prototrophic strains [48]. Briefly, the vector was linearized by digestion with *AsiSI* (Life Technologies) restriction endonuclease and nicked with *Nb.BsmI* (New England BioLabs). Synthetic DNA fragments were PCR-amplified - using forward primer FW_USER_TDH3 or FW_USER_PDA1 combined with reverse primer RV_USER_yeGFP - and subsequently cloned into the linearized vector backbone by uracil-excision based (USER) cloning technique [51,52]. Plasmids were transformed into *E. coli* for storage and amplification. Correct plasmid assembly was verified by PCR and Sanger sequencing (Eurofins Genomics) using primers ADH1_test_fw and CYC1_test_rv. Constructed integrative vectors (pLK0106 and pLK0107) were *NotI* (Life Technologies) digested to capture the linear fragments for integration. *S. cerevisiae* was transformed as previously described [53]. For genetic integration of cassettes, 1 µg of linear DNA was transformed into yeast for integration into the XII-1 chromosomal integration site [54]. Cells were plated onto selective YPD plates and colonies were re-streaked on selective plates. Genomic DNA was

extracted as previously described [55], and integration verified by PCR using XII-1_up and XII-1_down. All oligonucleotides used in this study can be found in the supplementary material (Table S1).

Fluorescence analysis

Fluorescence measurements of liquid cultures were conducted in black clear-bottomed 96-well microplates (Greiner Bio-One, Austria) using a SpectraMax iD3 multi-mode plate reader (Molecular Devices LLC, U.S.A). For fluorescence analysis of the fluorescent protein mCherry, endpoint measurements were recorded by setting the excitation wavelength at 580 nm and the emission wavelength at 620 nm. For liquid cultures, fluorescence intensities were normalized to the optical density measured at 600 nm (OD_{600}) using transparent flat-bottomed 96-well microplates (Greiner bio-one B.V., Netherlands). Prior to measurements of liquid cultures, cells were washed and four times concentrated.

For fluorescence analysis of the pH-sensitive protein mCherryEA, excitation scans were recorded by setting the excitation wavelength between 400 nm and 590 nm and the emission wavelength at 630 nm. For ratiometric analysis of the biosensor signal, the emission maxima obtained upon an excitation at 454 nm and 580 nm were taken and the corresponding biosensor ratio was calculated by dividing the former emission intensity by the latter as recently described[8]. For fluorescence analysis of the redox biosensor protein Mrx1-roGFP2, the calculation of Exc. 380 nm/ Exc. 470 nm (Em. 510 nm) was used for the determination of the biosensor ratio as recently described[16]. For determination of the biosensor oxidation degree (OxD), biosensor ratios from untreated samples were normalized to fully reduced (100 mM Dithiothreitol (DTT) in PBS buffer; pH 7.0) or oxidized (100 mM Natriumhypochlorite (NaOCl) in PBS buffer, pH 7.0) samples according to equation1. Here, $I380_{sample}$ and $I470_{sample}$ represent the

554 measured fluorescence intensities received for an excitation at 380 nm and 470 nm, respectively. Fully
555 reduced and oxidized controls are given by $I380_{red}$, $I470_{red}$ and $I380_{ox}$, $I470_{ox}$, respectively.

$$OxD = \frac{I380_{sample}\ x\ I470_{red} - I380_{red}\ x\ I470_{sample}}{I380_{sample}\ x\ I470_{red} - I380_{sample}\ x\ I470_{ox} + I380_{ox}\ x\ I470_{sample} - I380_{red}\ x\ I470_{sample}} \quad (1)$$

556

557

558 **Microplate reader-based analysis of sensor signals in colonies on agar plates**

559 Prior to robotic spotting of cell cultures, wells of 96-well microtiter plates (Greiner bio-one B.V.,
560 Netherlands) were filled with 200 µL overnight culture adjusted to an OD_{600} of 1 in the respective media.
561 For dilution series, the OD_{600} was set to 10 and 1:10 dilutions prepared in microtiter plates. The working
562 plate (96-well plate) was used as a source plate for robotic spotting using a ROTOR HDA benchtop robot
563 (Singer Instruments, United Kingdom) on rectangular OmniTray plates (Singer Instruments, United
564 Kingdom) with solidified medium on the target plate as recently described[8]. The OmniTray plates were
565 prepared by using 50 mL of the respective media supplemented with appropriate antibiotic and IPTG for
566 biosensor expression if required. Agar plates with spotted cell cultures in an arrayed format were
567 cultivated for 24 hours (*E. coli* and *S. cerevisiae* strains) or 48 hours for *C. glutamicum* strains if not
568 otherwise stated. Fluorescence analysis was performed using a SpectraMax iD3 multi-mode plate reader
569 (Molecular Devices LLC, U.S.A). Prior to fluorescence analysis, the lid from the OmniTray plate was
570 removed. A 96-well plate scheme was selected for the measurement mode and the wells selected for
571 targeting the respective colonies arrayed in a 96-well scheme on the agar plates. Measurement height
572 was set to 5 mm and measurements were performed at ambient temperature.

573

574

Fluorescence imaging of arrayed colonies

Fluorescence imaging of microbial colonies on agar plates was carried out using the photo-documentation system FUSION FX (Vilber Lourmat, France) and the FUSION FX EVOLUTION-CAPT software (Vilber Lourmat) for image analyses. For fluorescence analysis of the fluorescent protein mCherry, the FUSION FX was equipped with a capsule for excitation at 530 nm and an emission filter at 595 nm. For yeGFP analysis a capsule for excitation at 480 nm and a filter for emission 530 nm were used. Exposure time was set to 800 msec if not stated otherwise. Biosensor signals from the pH-sensitive protein mCherryEA were measured using the FUSION FX as recently described [8]. For fluorescence analysis using the Phenobooth (Singer Instruments, United Kingdom), the blue channel was selected for excitation (470 nm) and the emission intensity measured using a GFP filter (527 nm/ 20 nm).

White light imaging and determination of colony sizes

White light images were captured using the Phenobooth (Singer Instruments, United Kingdom). If required, images were processed prior to analyzing the images using Cellprofiler 4 (version 4.0.7) [56]. In order to determine colony sizes, the respective images were analyzed *via* the Python toolbox Pyphe [57].

Statistical analysis

Biosensor signals were analyzed using one-way variance (ANOVA) followed by Tukey´s test. The respective analysis was performed using Python 3 [58], and Pandas [59] was used to handle data frames. ANOVA was performed using the ols() and anova_lm() function of the statsmodels package [60]. Tukey´s

596 test was performed using tukey_hsd() function of the bioinfokit package [61]. Differences were considered

597 significant when p-value < 0.05. All data were plotted and visualized using the software Origin.

598 **Abbreviations**

CTAB	Cetyltrimethylammonium bromide
DTT	Dithiothreitol
EV	Empty vector
FRP	Fluorescent reporter protein
GFP	Green fluorescent protein
IPTG	Isopropyl β- d-1-thiogalactopyranoside
OD	Optical density
OxD	Oxidation degree
RBS	Ribosomal binding site
RFLU	Relative fluorescence units
roGFP2	Redox sensitive GFP2
TFB	Transcription factor-based biosensor
WT	Wild type

599

600 **Credit author statement**

601 **Fabian S. F. Hartmann:** Conceptualization; Data curation, Formal analysis, Investigation, Methodology,

602 Validation, Visualization, Writing of original draft; Writing-review & editing; **Tamara Weiß:**

603 Conceptualization; Data curation, Formal analysis, Investigation, Methodology, Validation, Visualization,

604 Writing of original draft; Writing-review & editing; **Louise L. B. Kastberg:** Formal analysis, Investigation,

605 Writing-review & editing; **Christopher T. Workman:** Funding acquisition, Writing-review & editing; **Gerd**

606 **M. Seibold:** Conceptualization; Funding acquisition; Supervision; Writing-original draft; Writing-review &

607 editing.

608

609 **Funding**

610 This work received funding by the Novo Nordisk Fonden within the framework of the Fermentation-

611 based Biomanufacturing Initiative (FBM) (FBM-grant: NNF17SA0031362) and from the Bio Based

Industries Joint Undertaking under the European Union´s Horizon 2020 research and innovation program (Grant agreement No 790507).

Availability of data and materials

All data generated and analyzed during this study are included in this article and its additional files. Raw datasets are available from the corresponding author on reasonable request.

Conflict of Interest

The authors declare that the research was conducted in the absence of any commercial or financial relationships that could be construed as a potential conflict of interest.

Acknowledgment

We would like to thank the Fermentation Core at DTU Bioengineering for excellent technical support.

References

(1) French, S.; Coutts, B. E.; Brown, E. D. Open-Source High-Throughput Phenomics of Bacterial Promoter-Reporter Strains. *Cell Syst.* **2018**, *7* (3), 339-346.e3. https://doi.org/10.1016/j.cels.2018.07.004.

(2) Nichols, R. J.; Sen, S.; Choo, Y. J.; Beltrao, P.; Zietek, M.; Chaba, R.; Lee, S.; Kazmierczak, K. M.; Lee, K. J.; Wong, A.; Shales, M.; Lovett, S.; Winkler, M. E.; Krogan, N. J.; Typas, A.; Gross, C. A. Phenotypic Landscape of a Bacterial Cell. *Cell* **2011**, *144* (1), 143–156. https://doi.org/10.1016/j.cell.2010.11.052.

(3) Liu, W.; Jiang, R. Combinatorial and High-Throughput Screening Approaches for Strain Engineering. *Appl. Microbiol. Biotechnol.* **2015**, *99* (5), 2093–2104. https://doi.org/10.1007/s00253-015-6400-0.

(4) Zeng, W.; Guo, L.; Xu, S.; Chen, J.; Zhou, J. High-Throughput Screening Technology in Industrial Biotechnology. *Trends Biotechnol.* **2020**, *38* (8), 888–906. https://doi.org/10.1016/j.tibtech.2020.01.001.

(5) Tanaka, Y.; Sasaki, N.; Ohmiya, A. Biosynthesis of Plant Pigments: Anthocyanins, Betalains and Carotenoids. *Plant J.* **2008**, *54* (4), 733–749. https://doi.org/10.1111/j.1365-313X.2008.03447.x.

(6) Peters, J. M.; Colavin, A.; Shi, H.; Czarny, T. L.; Larson, M. H.; Wong, S.; Hawkins, J. S.; Lu, C. H. S.; Koo, B. M.; Marta, E.; Shiver, A. L.; Whitehead, E. H.; Weissman, J. S.; Brown, E. D.; Qi, L. S.; Huang, K. C.; Gross, C. A. A Comprehensive, CRISPR-Based Functional Analysis of Essential Genes in Bacteria. *Cell* **2016**, *165* (6), 1493–1506. https://doi.org/10.1016/j.cell.2016.05.003.

(7) Kaczmarek, J. A.; Prather, K. L. J. Effective Use of Biosensors for High-Throughput Library Screening for Metabolite Production. *J. Ind. Microbiol. Biotechnol.* **2021**, *48* (9–10). https://doi.org/10.1093/jimb/kuab049.

(8) Hartmann, F. S. F.; Weiß, T.; Shen, J.; Smahajcsik, D.; Savickas, S.; Seibold, G. M. Visualizing the pH in *Escherichia coli* Colonies via the Sensor Protein mCherryEA Allows High-Throughput Screening of Mutant Libraries. *mSystems* **2022**, 2021.07.08.451719. https://doi.org/doi.org/10.1128/msystems.00219-22.

(9) Schallmey, M.; Frunzke, J.; Eggeling, L.; Marienhagen, J. Looking for the Pick of the Bunch: High-Throughput Screening of Producing Microorganisms with Biosensors. *Curr. Opin. Biotechnol.* **2014**, *26*, 148–154. https://doi.org/10.1016/j.copbio.2014.01.005.

(10) Ding, N.; Zhou, S.; Deng, Y. Transcription-Factor-Based Biosensor Engineering for Applications in Synthetic Biology. *ACS Synth. Biol.* **2021**, *10* (5). https://doi.org/10.1021/acssynbio.0c00252.

(11) Mahr, R.; Frunzke, J. Transcription Factor-Based Biosensors in Biotechnology: Current State and Future Prospects. *Appl. Microbiol. Biotechnol.* **2016**, *100* (1), 79–90. https://doi.org/10.1007/s00253-015-7090-3.

(12) Bermejo, C.; Haerizadeh, F.; Takanaga, H.; Chermak, D.; Frommer, W. B. Optical Sensors for Measuring Dynamic Changes of Cytosolic Metabolite Levels in Yeast. *Nat. Protoc.* **2011**, *6* (11), 1806–1817. https://doi.org/10.1038/nprot.2011.391.

(13) Martynov, V. I.; Pakhomov, A. A.; Deyev, I. E.; Petrenko, A. G. Genetically Encoded Fluorescent Indicators for Live Cell pH Imaging. *Biochim. Biophys. Acta - Gen. Subj.* **2018**, *1862* (12), 2924–2939. https://doi.org/10.1016/j.bbagen.2018.09.013.

(14) Martinez, K. A.; Kitko, R. D.; Mershon, J. P.; Adcox, H. E.; Malek, K. A.; Berkmen, M. B.; Slonczewski, J. L. Cytoplasmic pH Response to Acid Stress in Individual Cells of *Escherichia coli* and *Bacillus subtilis* Observed by Fluorescence Ratio Imaging Microscopy. *Appl. Environ. Microbiol.* **2012**, *78* (10), 3706–3714. https://doi.org/10.1128/AEM.00354-12.

(15) Depaoli, M. R.; Bischof, H.; Eroglu, E.; Burgstaller, S.; Ramadani-Muja, J.; Rauter, T.; Schinagl, M.; Waldeck-Weiermair, M.; Hay, J. C.; Graier, W. F.; Malli, R. Live Cell Imaging of Signaling and Metabolic Activities. *Pharmacol. Ther.* **2019**, *202*, 98–119. https://doi.org/10.1016/j.pharmthera.2019.06.003.

(16) Hartmann, F. S. F.; Clermont, L.; Tung, Q. N.; Antelmann, H.; Seibold, G. M. The Industrial Organism *Corynebacterium glutamicum* Requires Mycothiol as Antioxidant to Resist against Oxidative Stress in Bioreactor Cultivations. *Antioxidants* **2020**, *9* (10), 1–13. https://doi.org/10.3390/antiox9100969.

(17) Goldbeck, O.; Eck, A. W.; Seibold, G. M. Real Time Monitoring of NADPH Concentrations in *Corynebacterium glutamicum* and *Escherichia coli* via the Genetically Encoded Sensor mBFP. *Front. Microbiol.* **2018**, *9* (OCT), 1–10. https://doi.org/10.3389/fmicb.2018.02564.

(18) Hartmann, F. S. F.; Anastasiou, I.; Weiß, T.; Lkhaasuren, T. Combined Sensor-Based Monitoring of

Mycothiol Redox Potential and DNA-Damage Response in *Corynebacterium glutamicum*. *bioRxiv* **2022**. https://doi.org/https://doi.org/10.1101/2022.07.25.501298.

(19) Aguiar-Cervera, J. E.; Delneri, D.; Severn, O. A High-throughput Screening Method for the Discovery of Saccharomyces and Non- Saccharomyces Yeasts with Potential in the Brewing Industry . *Eng. Biol.* **2021**, *5* (3), 72–80. https://doi.org/10.1049/enb2.12013.

(20) Daniel, B.; Lawless, C. Modelling Competition for Nutrients between Microbial Populations Growing on a Solid Agar Surface. *bioRxiv* **2017**. https://doi.org/10.1101/086835.

(21) Hennessy, R. C.; Stougaard, P.; Olsson, S. A Microplate Reader-Based System for Visualizing Transcriptional Activity during *in Vivo* Microbial Interactions in Space and Time. *Sci. Rep.* **2017**, *7* (1). https://doi.org/10.1038/s41598-017-00296-4.

(22) Göttert, H.; Mattiazzi Usaj, M.; Rosebrock, A. P.; Andrews, B. J. Reporter-Based Synthetic Genetic Array Analysis: A Functional Genomics Approach for Investigating Transcript or Protein Abundance Using Fluorescent Proteins in *Saccharomyces cerevisiae*. In *Methods in Molecular Biology*; 2018; Vol. 1672. https://doi.org/10.1007/978-1-4939-7306-4_40.

(23) Entian, K. D.; Kötter, P. 25 Yeast Genetic Strain and Plasmid Collections. *Methods Microbiol.* **2007**, *36* (06), 629–666. https://doi.org/10.1016/S0580-9517(06)36025-4.

(24) Peng, B.; Williams, T. C.; Henry, M.; Nielsen, L. K.; Vickers, C. E. Controlling Heterologous Gene Expression in Yeast Cell Factories on Different Carbon Substrates and across the Diauxic Shift: A Comparison of Yeast Promoter Activities. *Microb. Cell Fact.* **2015**, *14* (1), 1–11. https://doi.org/10.1186/s12934-015-0278-5.

(25) Rajendran, M.; Claywell, B.; Haynes, E. P.; Scales, U.; Henning, C. K.; Tantama, M. Imaging pH Dynamics Simultaneously in Two Cellular Compartments Using a Ratiometric pH-Sensitive Mutant of mCherry. *ACS Omega* **2018**, *3* (8). https://doi.org/10.1021/acsomega.8b00655.

(26) Wilks, J. C.; Slonczewski, J. L. pH of the Cytoplasm and Periplasm of *Escherichia coli*: Rapid Measurement by Green Fluorescent Protein Fluorimetry. *J. Bacteriol.* **2007**, *189* (15), 5601–5607. https://doi.org/10.1128/JB.00615-07.

(27) Salmond, C. V.; Kroll, R. G.; Booth, I. R. The Effect of Food Preservatives on pH Homeostasis in *Escherichia coli*. *J. Gen. Microbiol.* **1984**, *130* (11), 2845–2850. https://doi.org/10.1099/00221287-130-11-2845.

(28) Padan, E.; Zilberstein, D.; Schuldiner, S. pH Homeostasis in Bacteria. *BBA - Rev. Biomembr.* **1981**, *650* (2–3), 151–166. https://doi.org/10.1016/0304-4157(81)90004-6.

(29) Piatkevich, K. D.; Malashkevich, V. N.; Almo, S. C.; Verkhusha, V. V. Engineering ESPT Pathways Based on Structural Analysis of LSSmKate Red Fluorescent Proteins with Large Stokes Shift. *J. Am. Chem. Soc.* **2010**, *132* (31), 10762–10770. https://doi.org/10.1021/ja101974k.

(30) Hartmann, F. S. F.; Anastasiou, I.; Weiß, T.; Shen, J.; Seibold, G. M. Impedance Flow Cytometry for Viability Analysis of *Corynebacterium glutamicum*. *J. Microbiol. Methods* **2021**, *191* (September), 106347. https://doi.org/10.1016/j.mimet.2021.106347.

(31) Reyes, A. M.; Pedre, B.; De Armas, M. I.; Tossounian, M. A.; Radi, R.; Messens, J.; Trujillo, M. Chemistry and Redox Biology of Mycothiol. *Antioxidants Redox Signal.* **2018**, *28* (6), 487–504. https://doi.org/10.1089/ars.2017.7074.

(32) Chi, B. K.; Busche, T.; Van Laer, K.; Bäsell, K.; Becher, D.; Clermont, L.; Seibold, G. M.; Persicke, M.; Kalinowski, J.; Messens, J.; Antelmann, H. Protein S-Mycothiolation Functions as Redox-Switch and Thiol Protection Mechanism in *Corynebacterium glutamicum* under Hypochlorite Stress. *Antioxidants Redox Signal.* **2014**, *20* (4), 589–605. https://doi.org/10.1089/ars.2013.5423.

(33) Liu, Y. B.; Long, M. X.; Yin, Y. J.; Si, M. R.; Zhang, L.; Lu, Z. Q.; Wang, Y.; Shen, X. H. Physiological Roles of Mycothiol in Detoxification and Tolerance to Multiple Poisonous Chemicals in *Corynebacterium glutamicum*. *Arch. Microbiol.* **2013**, *195* (6), 419–429. https://doi.org/10.1007/s00203-013-0889-3.

(34) Tung, Q. N.; Loi, V. Van; Busche, T.; Nerlich, A.; Mieth, M.; Milse, J.; Kalinowski, J.; Hocke, A. C.; Antelmann, H. Stable Integration of the Mrx1-roGFP2 Biosensor to Monitor Dynamic Changes of the Mycothiol Redox Potential in *Corynebacterium glutamicum*. *Redox Biol.* **2019**, *20*, 514–525. https://doi.org/10.1016/j.redox.2018.11.012.

(35) Si, M.; Xu, Y.; Wang, T.; Long, M.; Ding, W.; Chen, C.; Guan, X.; Liu, Y.; Wang, Y.; Shen, X.; Liu, S. J. Functional Characterization of a Mycothiol Peroxidase in *Corynebacterium glutamicum* That Uses Both Mycoredoxin and Thioredoxin Reducing Systems in the Response to Oxidative Stress. *Biochem. J.* **2015**, *469* (1), 45–57. https://doi.org/10.1042/BJ20141080.

(36) Pedre, B.; Van Molle, I.; Villadangos, A. F.; Wahni, K.; Vertommen, D.; Turell, L.; Erdogan, H.; Mateos, L. M.; Messens, J. The *Corynebacterium glutamicum* Mycothiol Peroxidase Is a Reactive Oxygen Species-Scavenging Enzyme That Shows Promiscuity in Thiol Redox Control. *Mol. Microbiol.* **2015**, *96* (6), 1176–1191. https://doi.org/10.1111/mmi.12998.

(37) Tossounian, M. A.; Pedre, B.; Wahni, K.; Erdogan, H.; Vertommen, D.; Van Molle, I.; Messens, J. *Corynebacterium diphtheriae* Methionine Sulfoxide Reductase a Exploits a Unique Mycothiol Redox Relay Mechanism. *J. Biol. Chem.* **2015**, *290* (18), 11365–11375. https://doi.org/10.1074/jbc.M114.632596.

(38) Si, M.; Zhao, C.; Zhang, B.; Wei, D.; Chen, K.; Yang, X.; Xiao, H.; Shen, X. Overexpression of Mycothiol Disulfide Reductase Enhances *Corynebacterium glutamicum* Robustness by Modulating Cellular Redox Homeostasis and Antioxidant Proteins under Oxidative Stress. *Sci. Rep.* **2016**, *6* (July), 1–14. https://doi.org/10.1038/srep29491.

(39) Navarrete, C.; Estrada, M.; Martínez, J. L. *Debaryomyces hansenii*: An Old Acquaintance for a Fresh Start in the Era of the Green Biotechnology. *World J. Microbiol. Biotechnol.* **2022**, *38* (6), 1–10. https://doi.org/10.1007/s11274-022-03280-x.

(40) Hartmann, F. S. F.; Udugama, I. A.; Seibold, G. M.; Sugiyama, H.; Gernaey, K. V. Digital Models in Biotechnology : Towards Multi-Scale Integration and Implementation. *Biotechnol. Adv.* **2022**, *60*, 108015. https://doi.org/10.1016/j.biotechadv.2022.108015.

(41) Bertani, G. Lysogeny at Mid-Twentieth Century: P1, P2, and Other Experimental Systems. *J. Bacteriol.* **2004**, *186* (3), 595–600. https://doi.org/10.1128/JB.186.3.595-600.2004.

(42) Studier, F. W.; Moffatt, B. A. Use of Bacteriophage T7 RNA Polymerase to Direct Selective High-Level Expression of Cloned Genes. *J. Mol. Biol.* **1986**, *189* (1), 113–130. https://doi.org/10.1016/0022-2836(86)90385-2.

(43) Blattner, F. R.; Plunkett, G.; Bloch, C. A.; Perna, N. T.; Burland, V.; Riley, M.; Collado-Vides, J.; Glasner, J. D.; Rode, C. K.; Mayhew, G. F.; Gregor, J.; Davis, N. W.; Kirkpatrick, H. A.; Goeden, M.

A.; Rose, D. J.; Mau, B.; Shao, Y. The Complete Genome Sequence of *Escherichia coli* K-12. *Science (80-.).* **1997**, *277* (5331), 1453–1462. https://doi.org/10.1126/science.277.5331.1453.

(44) Abe, S.; Takayama, K. I.; Kinoshita, S. Taxonomical Studies on Glutamic Acid-Producing Bacteria. *J. Gen. Appl. Microbiol.* **1967**, *13* (3). https://doi.org/10.2323/jgam.13.279.

(45) Eikmanns, B. J.; Kleinertz, E.; Liehl, W.; Sahm, H. A Family of *Corynebacterium glutamicum*/ *Escherichia coli* Expression and Promoter Probing. *Plasmid* **1991**, *102*, 93–98. https://doi.org/10.1016/0378-1119(91)90545-M.

(46) Jakoby, M.; Carole-Estelle; Ngouoto-Nkili; Burkovski, A. Construction and Application of New *Corynebacterium glutamicum* Vectors. *Biotechnol. Tech.* **1999**, *13* (6), 437–441. https://doi.org/10.1023/A:1008968419217.

(47) Shi, F.; Luan, M.; Li, Y. Ribosomal Binding Site Sequences and Promoters for Expressing Glutamate Decarboxylase and Producing γ-Aminobutyrate in *Corynebacterium glutamicum*. *AMB Express* **2018**, *8* (1). https://doi.org/10.1186/s13568-018-0595-2.

(48) Stovicek, V.; Borja, G. M.; Forster, J.; Borodina, I. EasyClone 2.0: Expanded Toolkit of Integrative Vectors for Stable Gene Expression in Industrial *Saccharomyces cerevisiae* Strains. *J. Ind. Microbiol. Biotechnol.* **2015**, *42* (11), 1519–1531. https://doi.org/10.1007/s10295-015-1684-8.

(49) Van der Rest, M. E.; Lange, C.; Molenaar, D. A Heat Shock Following Electroporation Induces Highly Efficient Transformation of *Corynebacterium glutamicum* with Xenogeneic Plasmid DNA. *Appl. Microbiol. Biotechnol.* **1999**, *52* (4). https://doi.org/10.1007/s002530051557.

(50) Cormack, B. P.; Bertram, G.; Egerton, M.; Gow, N. A. R.; Falkow, S.; Brown, A. J. P. Yeast-Enhanced Green Fluorescent Protein (yEGFP): A Reporter of Gene Expression in *Candida albicans*. *Microbiology* **1997**, *143* (2), 303–311. https://doi.org/10.1099/00221287-143-2-303.

(51) Nour-Eldin, H. H.; Geu-Flores, F.; Halkier, B. A. USER Cloning and USER Fusion: The Ideal Cloning Techniques for Small and Big Laboratories. In *Plant Secondary Metabolism Engineering*; 2010; Vol. 643, pp 185–200. https://doi.org/10.1007/978-1-60761-723-5.

(52) Jensen, N. B.; Strucko, T.; Kildegaard, K. R.; David, F.; Maury, J.; Mortensen, U. H.; Forster, J.; Nielsen, J.; Borodina, I. EasyClone: Method for Iterative Chromosomal Integration of Multiple Genes in *Saccharomyces cerevisiae*. *FEMS Yeast Res.* **2014**, *14* (2), 238–248. https://doi.org/10.1111/1567-1364.12118.

(53) Gietz, R. D.; Schiestl, R. H. High-Efficiency Yeast Transformation Using the LiAc/SS Carrier DNA/PEG Method. *Nat. Protoc.* **2007**, *2* (1), 31–34. https://doi.org/10.1038/nprot.2007.13.

(54) Mikkelsen, M. D.; Buron, L. D.; Salomonsen, B.; Olsen, C. E.; Hansen, B. G.; Mortensen, U. H.; Halkier, B. A. Microbial Production of Indolylglucosinolate through Engineering of a Multi-Gene Pathway in a Versatile Yeast Expression Platform. *Metab. Eng.* **2012**, *14* (2), 104–111. https://doi.org/10.1016/j.ymben.2012.01.006.

(55) Lõoke, M.; Kristjuhan, K.; Kristjuhan, A. Extraction of Genomic DNA from Yeasts for PCR-Based Applications. *Biotechniques* **2011**, *50* (5), 325–328. https://doi.org/10.2144/000113672.EXTRACTION.

(56) Stirling, D. R.; Swain-Bowden, M. J.; Lucas, A. M.; Carpenter, A. E.; Cimini, B. A.; Goodman, A. CellProfiler 4: Improvements in Speed, Utility and Usability. *BMC Bioinformatics* **2021**, *22* (1).

https://doi.org/10.1186/s12859-021-04344-9.

(57) Kamrad, S.; Rodríguez-López, M.; Cotobal, C.; Correia-Melo, C.; Ralser, M.; Bähler, J. Pyphe, a Python Toolbox for Assessing Microbial Growth and Cell Viability in High-Throughput Colony Screens. *Elife* **2020**, *9*. https://doi.org/10.7554/eLife.55160.

(58) Van Rossum, G.; Drake, F. L. *Python 3 Reference Manual*; CreateSpace: Scotts Valley, CA, 2009.

(59) McKinney, W. Data Structures for Statistical Computing in Python. In Proceedings of the 9th Python in Science Conference. In *Proceedings of the 9th Python in Science Conference*; 2010. https://doi.org/10.25080/majora-92bf1922-00a.

(60) Seabold, S.; Perktold, J. Statsmodels: Econometric and Statistical Modeling with Python. In *Proceedings of the 9th Python in Science Conference*; 2010. https://doi.org/10.25080/majora-92bf1922-011.

(61) Bedre, R. Reneshbedre/Bioinfokit: Bioinformatics Data Analysis and Visualization Toolkit. Zenodo 2021. https://doi.org/10.5281/zenodo.4422035.